Catalysis Science & Technology

Accepted Manuscript

ROYAL SOCIETY OF CHEMISTRY

www.rsc.org/catalysis

Journal Name

ARTICLE

Promotional effect of iron oxide on the catalytic properties of Fe-MnO_x/TiO_2 (Anatase) Catalysts for the SCR reaction at low temperatures

Received 00th January 20xx,
Accepted 00th January 20xx

DOI: 10.1039/x0xx00000x

www.rsc.org/

Shengcai Deng,[a] Ke Zhuang,[a,b] Boliang Xu,[a] Yuanhua Ding,[c] Lei Yu,*[a,c] and Yining Fan*[a]

The surface ineraction of iron-improved MnO_x/TiO_2 (anatase) catalyst for the selective catalytic reduction of nitric oxide was studied by detailed experiments. It was found that iron improved the catalyst by regulating the polymerization degree and the dispersion of Mn oxide species supported on the anatase surface, which was the key factor for both of the SCR activity and the N_2 selectivity. The increased NO conversion was caused by higher Mn oxide dispersion while the selectivity evaluation showed that N_2O formation on MnO_x/TiO_2 catalyst was much higher than that on the iron-improved catalyst. Isotopic labelled experiments of $^{15}NH_3$ with NO indicated that NH was the key species for N_2O generation. NH was easily to be generated on MnO_x/TiO_2 without iron, which had higher oxidability than iron-improved catalyst, as identified by the temeperature programmed reduction of H_2 experiments.

Introduction

Nitric oxide (NO) is one of the major air pollutants in atmospheric environment that cause acidic rain, photochemical smog, ozone depletion, greenhouse effect, *etc*.[1] Therefore, elimination of NO is a practical research topic with imperious demands.[1-6] Recently, manganese oxide (MnO_x)-based catalysts have attracted much attention in this area because of their unique activities in the selective catalytic reduction (SCR) of NO with NH_3 to harmless N_2 at low temperature.[2-4] Previous studies have shown that among the anatase-supported MnO_x catalysts prepared through different methods, MnO_x/TiO_2, prepared through the sol-gel method, exhibited higher activities than others that were fabricated through wet-impregnations or co-precipitations.[3] However, the major defect of these NO elimination technologies is the generation of N_2O, which is the product of the insufficient reduction of NO and the oxidation of NH_3.

During the investigations in the field, iron has been found to be an effective element to improve the catalytic properties.[4-6] In 2003, Yang *et. al.* reported that impregnated the Fe-MnO_x/TiO_2 catalysts not only have elevated activities for NO-SCR, but also obviously restricted N_2O generation, and they attributed these promoting effects to the lower crystallinity of manganese oxide induced by iron oxide.[4h] Wu *et. al.* then proposed that the addition of iron resulted in the amorphous MnO_x instead of the crystalline, leading to higher SCR activity of Fe-MnO_x/TiO_2 catalyst.[4g] Recently, Dong *et. al.* found that addition of surfactant cationic surfactant cetyltrimethyl ammonium bromide (CTAB) could suppress the transformation of anatase to rutile in Fe-MnO_x/TiO_2 catalyst and obviously increase its SCR activity.[4d] Since MnO_x was the active component for the low-temperature SCR, previous reports have also pointed out that its dispersion state on supporters was the key factor for SCR performance and Smirniotis *et. al.* has proposed that the aggregation morphology of MnO_x affected the catalyst activity much[5] while Bliek group's work disclosed that aggregated MnO_x species accelerated N_2O generation.[6] But there are still several basic mechanism problems unresolved in the field and the relationships of iron with the MnO_x dispersion state as well as the catalyst activity and the reaction selectivity are still unclear. Our group aimed to develop green technologies with industrially applicable potential.[7] In order to reveal the intrinsic effects of iron promoter in the Fe-MnO_x/TiO_2 catalysts for further development, we have investigated the surface interaction among Fe-MnO_x/TiO_2. The experimental results have shown that iron improved the catalyst by regulating the polymerization degree and the dispersion of MnO_x species supported on the anatase surface, which was the key factor for both of the SCR activity and the N_2 selectivity. Herein, we wish to report our findings.

[a] *Key Laboratory of Mesoscopic Chemistry of MOE, Jiangsu Key Laboratory of Vehicle Emissions Control, Jiangsu Provincial Key Laboratory of Nanotechnology, School of Chemistry and Chemical Engineering, Nanjing University, Nanjing 210093, China. Email: ynfan@nju.edu.cn; Fax: +86-25-83317761; Tel: +86-25-83594620*
[b] *Environmental Engineering Research Sub-institute, State Power Science and Technology Research Institute, Nanjing 210031, China.*
[c] *Jiangsu Key Laboratory of Environmental Material and Environmental Engineering, School of Chemistry and Chemical Engineering, Yangzhou University, Yangzhou, 225002, China. Email: yulei@yzu.edu.cn; Fax: +86-514-87975244; Tel: +86-136-65295901*

Results and Discussion

We initially tested the catalytic activities of Fe(1.0)-MnO_x/TiO_2, MnO_x/TiO_2 and FeO_x/TiO_2 in SCR. As shown in Figure 1, the reactions proceeded quickly and reached a steady-state within 30 min. In comparison, the catalyst Fe(1.0)-MnO_x/TiO_2 obviously showed much higher activity than simple MnO_x/TiO_2 (Figure 1A, curves *a vs. b*) and the NO conversion reached 88 % at the highest value. But the catalyst FeO_x/TiO_2 was almost ineffective and the related NO conversions were just around 5 mol % (Figure 1A, curve *c*). The addition of iron also improved the N_2 selectivity of the SCR of NO (Figure 1B, curves *a vs. b*). Obviously, the iron component in the Fe-MnO_x/TiO_2catalysts acted as a promoter for the catalytic active component of MnO_x supported on anatase.

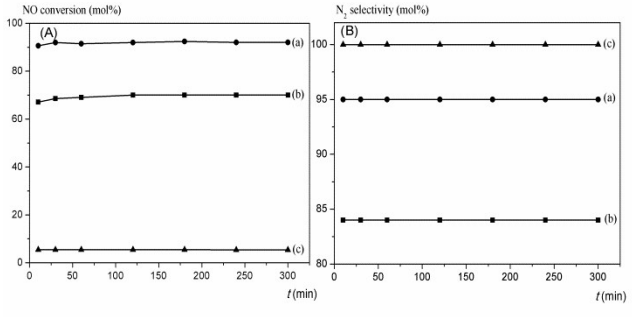

Figure 1 Catalyst activity test at 160 °C with GHSV at 1.0×10^5 h^{-1}: (*a*) Fe(1.0)-MnO_x/TiO_2; (*b*) MnO_x/TiO_2; (*c*) FeO_x/TiO_2[8]

To further disclose the role of iron in catalyst, a series of Fe-MnO_x/TiO_2 catalysts with different Fe/Ti ratio were then evaluated. As shown in Figure 2(A), for all catalysts, the NO conversions rose along with the reaction temperature, and reached a maximum at around 200 °C. Addition of iron benefited the NO conversion and the Fe(0.5)-MnO_x/TiO_2 was screened out to be the best catalyst (curve *c*). It was obvious that the iron-doped catalysts improved the reaction much at low temperature (80-160 °C), while no more than 10 mol% of the NO conversion was enhanced at high temperature (200-280 °C). Figure 2(B) disclosed that the N_2 selectivity was enhanced along with the Fe/Ti ratio increasing. Thus, it is obvious that the addition of iron not only enhanced that catalyst activity, but also restrained N_2O generation and increased N_2 selectivity.

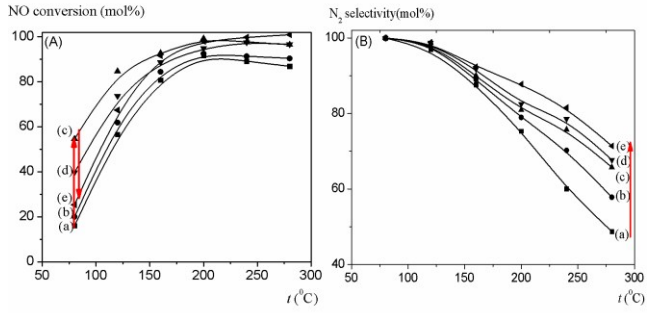

Figure 2 Catalyst evaluation in 30 min with GHSV at 1.0×10^5 h^{-1}: (*a*) MnO_x/TiO_2; (*b*) Fe(0.25)-MnO_x/TiO_2; (*c*) Fe(0.5)-MnO_x/TiO_2; (*d*) Fe(0.75)-MnO_x/TiO_2; (*e*) Fe(1.0)-MnO_x/TiO_2.

The transmission electron microscopy (TEM) and scanning electron microscopy (SEM) results indicated that the addition of iron resulted in much looser morphology of the catalyst material (Figure 3, Figure S3). In TEM and SEM images, the MnO_x/TiO_2 behaved as an aggregated massive solid (Figure 3A, Figure S3b,), but for Fe(1.0)-MnO_x/TiO_2, the material was segregated in much smaller pieces with loosen morphology (Figure 3B, Figure S3d). Further electron diffraction spectra (EDS) mapping technologies illustrated that both iron and manganese distributed uniformly in TiO_2 and the addition of iron undoubtedly avoided the aggregation of manganese oxide crystalline (Figure 3B-Mn *vs.* 3A-Mn).

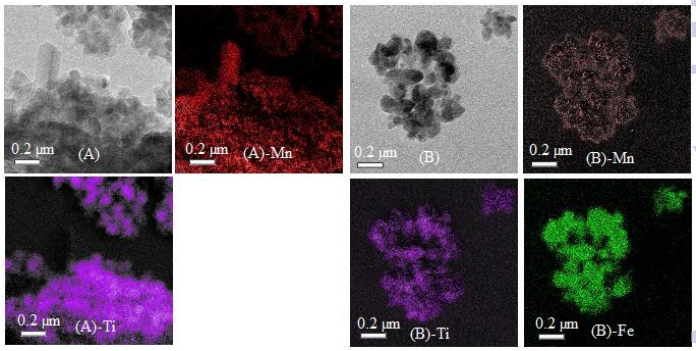

Figure 3 TEM image and element mapping of (A) MnO_x/TiO_2, (B) Fe(1.0)-MnO_x/TiO_2[9]

Table 1 calculated the TiO_2 crystallite size (D) at the Ti (101) lattice plane (29.4°) through Debye-Scherrer method. It was shown that the addition of iron and manganese led to smaller TiO_2 crystallite size, possibly because of its inhibitory effect for TiO_2 crystalline particle growth (Table 1, entries 2-6 *vs.* 1). The phenomena was well consistent with the references, which reported that the incorporation of Mn^{4+} and Fe^{3+} into the lattice restrained the growth of TiO_2.[10] It was interesting that although the TiO_2 sizes were gradually reduced with the increase of iron content, the surface area of the catalyst got its peak when Fe/Mn ratio reached 0.5 and the highest rate constant and turn over frequency (TOF) for NO conversion at 80 °C were also achieved at this Fe/Mn value (Table 1, entry 4 *vs.* 2-3 and 5-6). In order to explain the phenomenon, X-ray powder diffraction (XRD) analyses of the catalysts were performed. As shown in the XRD spectra (Figure 4), no MnO_2 signal (2Θ = 33.3 43.7 50.1 66.7°) was observed in the MnO_x/TiO_2 catalysts, indicating that MnO_x should be highly dispersed or exist in amorphous state. The crystalline Fe_2O_3 peak emerged when the Fe/Mn ratio was more than 0.5, and the BET surface area began to decrease. Besides, the addition of iron also affected the total amounts of acidic sites on catalyst surface (Table 1), which increased first by the enhanced catalyst dispersion but decreased then due to the Fe_2O_3 crystalline covering. The total acidity on catalyst surface is known to be the key point for the adsorption of NH_3, which is crucial for the selective reduction of NO. The peaks of desorption around 200 °C were assigned to the chemical adsorbed NH_3 on Lewis acid sites caused by MnO_x species(Figure S5), the adsorbed NH_3 species on MnO_x can then react with gaseous NO to give N_2 formation through the Eley–Rideal mechanism at low temperatures.[1j,12] Among

tested catalysts, Fe(0.5)-Mn/TiO_2 had the highest total acidity, as calculated from NH_3-temperature programmed desorption (TPD) results (Figure 5), and thus behaved the best catalytic activity for NO elimination (Table 1, entry 4).

Table 1 Physicochemical Properties of the Catalysts

entry	cat.[a]	D^b	A[c]	t.a.[d]	Mn/Ti[e]	k^f	TOF[g]
1	TiO_2	150	56	-	-	-	-
2	(I)	80	143.8	2.86	0.36	6.03	0.67
3	(II)	56	190.8	2.94	0.38	6.64	1.07
4	(III)	53	200.0	3.21	0.42	25	3.08
5	(IV)	38	154.2	3.04	0.49	23	2.53
6	(V)	n.d.[h]	149.7	2.75	0.51	15	1.74

[a] Catalyst: (I) MnO_x/TiO_2, (II) Fe(0.25)-MnO_x/TiO_2, (III) Fe(0.5)-MnO_x/TiO_2, (IV) Fe(0.75)-MnO_x/TiO_2, (V) Fe(1.0)-MnO_x/TiO_2. [b] Crystalline size of TiO_2 by $D_{(101)}$ (Å). [c] BET surface area (m^2/g). [d] Total NH_3-TPD peak area (a.u.). [e] Molar ratio of Mn/Ti on catalyst surface detected by XPS. [f] Rate constant for NO conversion at 80 °C ($mol \cdot m^{-2} \cdot s^{-1} \times 10^{-8}$). [g] Turn over frequency for NO conversion at 80 °C ($s^{-1} \times 10^{-4}$). [h] No obvious crystalline TiO_2 detected.

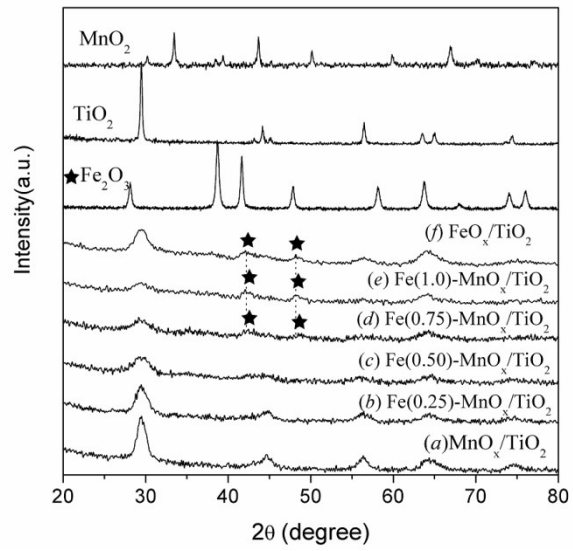

Figure 4 XRD analysis of the catalysts.[11]

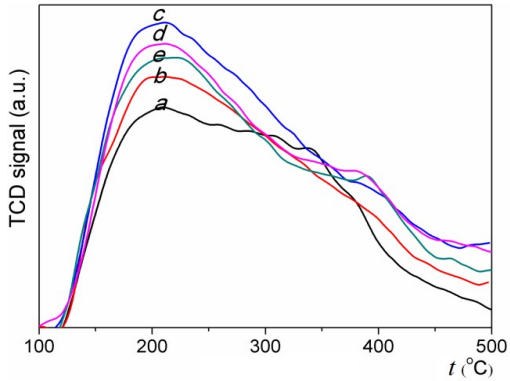

Figure 5 NH_3-TPD profile of the catalysts (*a*)MnO_x/TiO_2; (*b*) Fe(0.25)-MnO_x/TiO_2; (*c*) Fe(0.5)-MnO_x/TiO_2; (*d*) Fe(0.75)-MnO_x/TiO_2; (*e*) Fe(1.0)-MnO_x/TiO_2

The X-ray photoelectron spectroscopy (XPS) experiments were also used to investigate the chemical state of catalyst surface components. As shown in Figure S4,[9] the valence of Ti in the supporter did not change and the peaks around 457.6 and 463.4 eV were in correspondence to the signals of Ti2p3/2 and Ti2p1/2, which were characteristic peaks of Ti^{4+}. The additive iron mainly existed as Fe^{3+}, which was indicated by the overwhelming peak at 711.9 eV.[10] The valences of manganese were not affected by the addition of iron, and Mn^{4+} was the major species. Besides the lattice oxygen (O1s, 529.5 eV), the materials also contained absorbed oxygen, which was clearly characterized by the O1s signal at 531.0 eV. The Mn/Ti ratios on catalyst surfaces were then calculated according to the XPS analysis results (Table 1). It was very clear that the addition of iron led to the increase of Mn/Ti ratio on surface, which benefited the SCR of NO. But the sustained growing trend of Mn/Ti was not completely in agreement with the reaction rate constant and TOF, which reached the highest value with Fe(0.5)-MnO_x/TiO_2 (Table 1, entry 4). Therefore, it was suggested that the catalyst activity was also related with the dispersed state of MnO_x on surface.

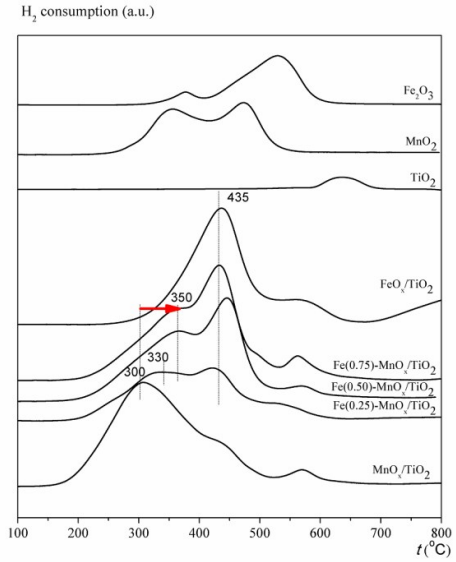

Figure 6 The H_2-TPR results of the catalysts

Temperature-programmed reduction (TPR) experiments with H_2 were then taken to confirm the MnO_x dispersion state on catalyst surface. As shown in Figure 6, there were two reduction peaks of H_2 consumption for MnO_x/TiO_2 catalyst: the broad peak around 200-500 °C indicated the reduction of Mn^{4+} to Mn^{2+}, while the peak at 580 °C was the characteristic for the reduction of Ti^{4+} to Ti^{3+} (curve *a*). The addition of iron led to a new peak around 430 °C, which was suggested to be the signal of the Fe_2O_3 reduction on TiO_2 surface (curves *b*-*e*). Obviously, the characteristic peak for MnO_x reduction shifted to higher temperature along with the increase of iron content (curves *b*-*e* *vs.* *a*), which indicated the decrease of its reducibility. It has been well-known that the highly dispersed MnO_x species has lower reducibility than aggregated MnO_x species.[13-14] Thus, from the above TPR results, it could be concluded that the addition of iron led to the formation of highly dispersed MnO_x

species on TiO_2. Among dispersed MnO_x species, the oligomers were more activated than the highly dispersed insular MnO_x for NO reduction.[13] Hence, the observed rate constants and TOF of the reactions were improved after the addition of iron, which might lead to the MnO_x oligomers at the first step (Table 1, entries 2-4). But the excess iron led to the highly dispersed insular MnO_x species, which resulted in the lower catalytic activity for NO reduction,[12] as shown in Table 1, entries 4-6.

The mechanisms for the generation of N_2O were our next concern. Thus, isotopic-labeled temperature-programmed surface reaction (TPSR) experiments using ^{14}NO and $^{15}NH_3$ were then employed to provide essential hints. As depicted in Figure 7, in the reactions catalyzed by MnO_x/TiO_2, $^{15}N^{14}NO$ was detected when the TPSR temperature reached 145 °C, indicating that the generation of N_2O from the reaction of NH_3 with NO started at this temperature. The oxidation of NH_3 by air began at 225 °C, where the characteristic $^{15}N^{15}NO$ signal was observed. But for the reactions using Fe(1.0)-MnO_x/TiO_2 catalyst, the generation of $^{14}N^{15}NO$ and $^{15}N^{15}NO$ both needed higher temperature, which were at 180 °C and 240 °C respectively. Besides, the *in situ* diffuse reflectance infrared Fourier transform spectra (DRIFT) also indicated that the addition of Fe restrained N_2O generation. As shown in Figure S5,[9] for MnO_x/TiO_2, the characteristic peak of N_2O emerged at 160 °C; But for Fe(1.0)-MnO_x/TiO_2, no N_2O signal was observed at the temperature lower than 200 °C.

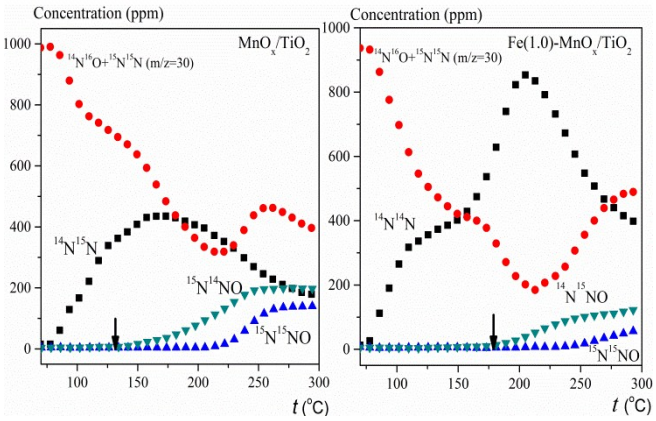

Figure 7 Isotopic-labeled TPSR experimental results for the reaction of ^{14}NO with $^{15}NH_3$.[15]

The reported works have illustrated that the NH_3 oxidation procedures affected the selectivity of the NO elimination reactions:[4d, 16] The oxidation of NH_3 afforded NH_2 (eq. 1), which led to N_2 through the reaction with NO (eq. 2) or dimerization (eq. 3). But the deep oxidation of NH_3 might generate NH (eq. 4), which led to undesired byproduct N_2O through the reaction with NO (eq. 5) or O^{2-} (eqs. 6-7). [4d, 16]

N_2 generation:

$NH_3 \xrightarrow[-H^+]{-e} NH_2$ (1)

$NH_2 + NO \longrightarrow N_2 + H_2O$ (2)

$2\,NH_2 \xrightarrow[-4H^+]{-4e} N_2$ (3)

VS

N_2O generation:

$NH_3 \xrightarrow[-2H^+]{-2e} NH$ (4)

$NH + NO \xrightarrow[-H^+]{-e} N_2O$ (5)

$NH + O^{2-} \xrightarrow{-2e} HNO$ (6)

$2HNO \longrightarrow N_2O + H_2O$ (7)

Therefore, the selectivity of the reaction might be controlled by the catalyst oxidability versus NH_3. The results of TPR experiments with H_2 showed that the addition of iron led to dispersed MnO_x species (Figure 6), which had low oxidability and thus avoided the generation of N_2O.[6] The TPSR experiments for the reaction of NH_3 with O_2 on the catalyst surface further supported our hypothesis. As shown in Figure 8, the NH_3 consumptions on Fe(1.0)-MnO_x/TiO_2 were obviously lower than that on MnO_x/TiO_2 (Image *a*) , indicating the much lower catalytic activity for NH_3 oxidation, which resulted in the high N_2 selectivity (Image *b*) and restrained the generation of over oxidation products N_2O and NO (Images *c*-*d*).

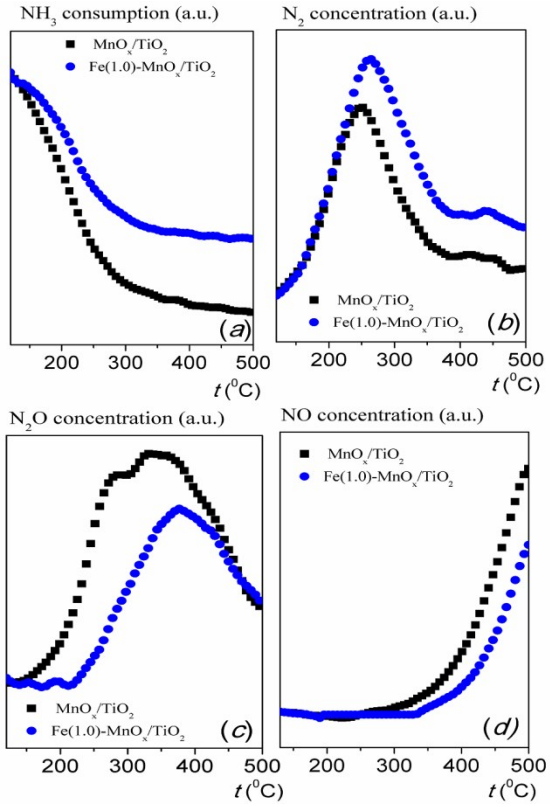

Figure 8. TPSR experimental results for the reaction of NH3 with O_2 (Reaction conditions: 2000 ppm NH_3, 4 vol.% O_2 balanced by Ar, GHSV = 1.0×10^5 h^{-1})

Experimental Section

Catalyst Preparation

The Fe-MnO_x/TiO_2 catalysts were prepared by sol-gel method: 48 ml butyl titanate was added into a vigorously stirred aqueous solution containing 126 ml *n*-butanol, 14 ml acetic acid, 12 ml deionized water and required amount of ferric nitrate and manganese nitrate (Mn/Ti molar ratio= 0.4, Fe/Mn molar ratio = 0.0 ~ 1.0). The obtained gel was aged for 24 h and dried at 110 °C, then calcined at 500 °C in air for 4 h. The prepared samples were crushed and sieved to 20-40 mesh. For comparison, MnO_2 and Fe_2O_3 catalysts prepared by decomposition of the corresponding nitrates under air at 300 °C and 500 °C for 4h, respectively.

Catalyst Characterization

Transmission electron microscopy (TEM) and electron diffraction spectra (EDS) were used to investigate the microstructure and the element dispersion of the catalyst with JEM-2010 UHR transmission electron microscope (TEM) operated at 200 KV.

Scanning electron microscope (SEM) experiments were performed with a Hitachi S-4800 electron microscope. The samples were vapor-deposited with gold before observation.

X-ray diffraction(XRD) studies were performed on a Bruker D8 ADVANCE Powder X-ray diffractometer equipped with Co Kα radiation (λ = 1.7026 Å). The X-ray tube was operated at 40 kV and 40 mA.

The surface areas of samples were determined by the BET isotherms of N_2 adsorption at -196 ^{0}C using a Micrometritics ASAP 2020 instrument with a auto-controlled system. 0.1g of catalyst was degassed at 300 ^{o}C for 2h before each measurement.

Ammonia temperature programmed desorption (NH_3-TPD) was performed in a quartz U-tube reactor, and 0.1 g catalyst powders were pretreated with argon flow (40 ml/min) at 500 ^{o}C for 1 h, and purged at 100 ^{o}C for 0.5 h, then heated from 100 to 500 ^{o}C at a heating rate of 10 ^{o}C /min. The desorbed NH_3 signal was measured by a thermal conductivity detector (TCD).

X-ray photoelectron spectroscopy (XPS) measurement was carried out using Multilab 2000 XPS system with a monochromatic Mg Kα source and a charge neutralizer. All the binding energy were referenced to the surface contaminated carbon (C1s=284.6 eV).

Hydrogen Temperature Programmed Reduction (H_2-TPR) were performed in a quartz U-tube reactor, and 0.05 g catalyst were reduced without pretreatment. The H_2 consumption signal was detected by a thermal conductivity detector (TCD).

Isotopic labeled $^{15}NH_3$+^{14}NO+O_2 Temperature programmed reaction were performed in a quartz U-tube reactor. 0.1 g of catalysts were pretreated in argon flow at 500 ^{o}C for 30min. Then, the catalysts were switched to argon flow containing 1000 ppm ^{14}NO, 1100ppm $^{15}NH_3$ with 4 vol. % O_2 and heated from 100-500 ^{o}C at the heating rate of 10 ^{o}C/min. The signals of ^{14}NO (m/z=30), $^{14}N_2O$ (m/z=44), $^{14}N^{15}NO$ (m/z=45), $^{15}N^{15}NO$ (m/z=46) and $^{14}N^{15}N$ (m/z=29), $^{14}N^{14}N$ (m/z=28) were measured by a quadrapole mass spectrometer.

In situ DRIFT spectra of absorbed and oxidized species of NH_3 were collected on a Nicolet 5700 FTIR instrument (4 cm^{-1} resolution) equipped with a gas flow system. Before measurement, the catalysts were pretreated for in N_2 flow for 0.5 h at 300 ^{o}C. After cooling to room temperature, the samples were exposed to NH_3 (1 vol. %)/N_2 for 0.5 h and purged by pure N_2 for 0.5 h. Then, the samples were heated to 300 ^{o}C with a linear heating rate (10 ^{0}C /min) in N_2+O_2 (1 vol. %) flow. The final DRIFT-IR spectra were recorded at different temperatures with subtraction of corresponding background spectra.

NH_3+O_2 temperature-programmed surface reaction (TPSR) were performed in a quartz U-tube reactor, 0.1 g catalysts were pretreated in argon flow at 500 ^{o}C for 1 h. Then the catalysts were switched to argon flow containing 2000 ppm of NH_3, 4 vol. % O_2 and heated from 100 to 500 ^{o}C at a heating rate of 10 ^{o}C/min. The signals of NO (m/z=30), NH_3 (m/z=17), N_2O (m/z=46) and N_2 (m/z=28) were measured by a quadrapole mass spectrometer.

Catalytic Performance test

Selective catalytic reduction (SCR) of NO by NH_3 was carried out in a fixed-bed U-tube glass reactor (i. d. 6 mm) with 0.1g catalyst samples. The inlet concentrations of reactants were 1000 ppm NO_x, 1100 ppm NH_3 and 4 % vol. O_2 and N_2 was the remainder. The catalytic reaction was carried out at 80-280 ^{o}C and 0.1 Mpa with a total flow rate of 3.1 ml s^{-1} (ambient conditions). The temperature of the catalyst was measured and controlled by means of a K-Type thermocouple (o.d.= 0.5 mm) attached closely to the catalyst bed. The NO (m/z = 30) and N_2O (m/z = 46) concentrations before and after reaction were determined by using a Quadrapole mass spectrometer (DycorDymaxion DM300M, AMETEK). Because the NO_2 gas was not found both of inlet and outlet reaction gas under the above SCR reaction conditions over MnO_x/TiO_2 catalyst activity test, the definitions used for NO conversion and N_2 selectivity are as follows:

$$\text{NO conversion} = 100 \times \frac{[NO]_{in} - [NO]_{out}}{[NO]_{in}}$$

$$N_2 \text{ selectivity} = 100 \times (1 - \frac{2[N_2O]}{[NO]_{in} - [NO]_{out}})$$

While working in excess oxygen and with NH_3/NO (molar ratio) ≥1, the NO conversion rate for the SCR process can be supposed to first order reaction model in NO. The rate constant *k* based on the specific surface area of sample was calculated according to the expression below:

$$k = -\frac{F_{in}}{m \times S} \ln(1 - x)$$

The NO turnover frequencies (NO TOFs) were calculated assuming a first-order reaction rate and according to the expression below:

$$\text{NO TOFs} = \frac{F_{in} - F_{out}}{M_{site}}$$

Where *k* is the rate constant based on BET surface area of sample ($mol \cdot m^{-2} \cdot s^{-1}$), NO TOFs is defined as the number of moles of NO converted per mole of active sites per second ($mol_{NO\ converted}/(mol_{site}s)$), F is the molar NO feed rate (mol s^{-1}), *m* is the catalyst mass (g), *S* is the specific surface area of catalyst sample (m^2 g^{-1}), *x* is the fractional NO conversion, M_{site} is the moles of catalytically active manganese species calculated by assuming all Mn component is catalytically active.

Conclusions

In conclusion, iron improved the catalyst by regulating the polymerization degree and dispersion state of MnO_x on its surface: The addition of iron led to the dispersed oligomerized MnO_x, which enhanced the total acidity on catalyst surface and thus improved its activity. The oligomerized MnO_x had lower oxidability versus NH_3 than the original polymerized one, and could restrain the deeply oxidized species NH, which was the key intermediate to generate the undesired byproduct N_2O. The excess iron addition led to the highly dispersed insular Mn

species with reduced oxidability, which benefited the SCR selectivity, but decreased the catalyst activity. Although this mechanism remains to be fully clarified and alternative processes may also exist, the conclusion should be the most likely mechanism based on the above experimental findings and the related literatures.

Acknowledgements

We thank Specialized Research Fund for the Doctoral Program of Higher Education (SRFDP-20120091111001), NNSFC (21202141, 21173182), the Opening Foundation of the Key Laboratory of Environmental Materials and Engineering of Jiangsu Province (K14010), Key Science & Technology Specific Projects of Yangzhou (YZ20122029) and Yangzhou Nature Science Foundation (YZ2014040) for financial support.

Notes and references

1. (*a*) B. Mu, J. Zhang, T. P. McNicholas, N. F. Reuel, S. Kruss and M. S. Strano, *Acc. Chem. Res.*, 2014, **47**, 979; (*b*) S. Zhang, H. Chen, Y. Xia, N. Liu, B. Lu and W. Li, *Appl. Microbiol. Biot.*, 2014, **98**, 8497; (*c*) P. Granger and V. I. Parvulescu, *Chem. Rev.*, 2011, **111**, 3155; (*d*) A. Zellner, R. Suntz and O. Deutschmann, *Angew. Chem. Int. Ed.*, 2015, **54**, 2653; (*e*) T. V. W. Janssens, H. Falsig, L. F. Lundegaard, P. N. R. Vennestrøm, S. B. Rasmussen, P. G. Moses, F. Giordanino, E. Borfecchia, K. A. Lomachenko, C. Lamberti, S. Bordiga, A. Godiksen, S. Mossin and P. Beato, *ACS Catal.*, 2015, **5**, 2832; (*f*) Y. Yu, Y. Li, X. Zhang, H. Deng, H. He and Y. Li, *Environ. Sci. Technol.*, 2015, **49**, 481; (*g*) J. Liu, Q. Zhao, X. Li, J. Chen and D. Zhang, *Appl. Catal. B-Environ.*, 2015, **165**, 519; (*h*) Z. Qu, L. Miao, H. Wang and Q. Fu, *Chem. Commun.*, 2015, **51**, 956; (*i*) A. Boubnov, H. W. P. Carvalho, D. E. Doronkin, T. Günter, E. Gallo, A. J. Atkins, C. R. Jacob and J.-D. Grunwaldt, *J. Am. Chem. Soc.*, 2014, **136**, 13006; (*j*) S. Xiong, Y. Liao, H. Dang, F. Qi and S. Yang, *RSC Adv.*, 2015, **5**, 27785; (*k*) L. Zhang, D. Zhang, J. Zhang, S. Cai, C. Fang, L. Huang, H. Li, R. Gao and L. Shi, *Nanoscale*, 2013, **5**, 9821; (*l*) W. Shan and H. Song, *Catal. Sci. Technol.*, 2015, **5**, 4280; (*m*) M. Fu, C. Li, P. Lu, L. Qu, M. Zhang, Y. Zhou, M. Yu and Y. Fang, *Catal. Sci. Technol.*, 2014, **4**, 14.
2. (*a*) S. Xiong, Y. Liao, X. Xiao, H. Dang and S. J. Yang, *Phys. Chem. C*, 2015, **119**, 4180; (*b*) J. Zhu, H. Li, L. Zhong, P. Xiao, X. Xu, X. Yang, Z. Zhao, J. Li, *ACS Catal.*, 2014, **4**, 2917; (*c*) E. Park, M. Kim, H. Jung, S. Chin and J. Jurng, *ACS Catal.*, 2013, **3**, 1518; (*d*) W. Wang, G. McCool, N. Kapur, G. Yuan, B. Shan, M. Nguyen, U. M. Graham, B. H. Davis, G. Jacobs, K. Cho and X. Hao, *Science*, 2012, **337**, 832; (*e*) J. E. Parks II, *Science*, 2010, **327**, 1584; (*f*) C. H. Kim, G. Qi, K. Dahlberg and W. Li, *Science*, 2010, **327**, 1624; (g) W. S. Kijlstra, D. S. Brands, H. I. Smit, E. K. Poels and A. Bliek, *J. Catal.*, 1997, **171**, 219; (h) Y. Liu, J. Xu, H. Li, S. Cai, H. Hu, C. Fang, L. Shi and D. Zhang, *J. Mater. Chem. A*, 2015, **3**, 11543.
3. (*a*) P. R. Ettireddy, N. Ettireddy, T. Boningari, R. Pardemann, and P. G. Smirniotis, *J. Catal.*, 2012, **292**, 53; (*b*) B. Jiang, Y. Liu and Z. Wu, *J. Hazard Mater.*, 2009, **162**, 1249.
4. (*a*) S. S. R. Putluru, L. Schill, A. D. Jensen, B. Siret, F. Tabaries and R. Fehrmann, *Appl. Catal. B-Environ.*, 2015, **165**, 628; (*b*) J. Li, C. Yang, Q. Zhang, Z. Li and W. Huang, *Catal. Commun.*, 2015, **62**, 24; (*c*) F. Cao, S. Su, J. Xiang, P. Wang, S. Hu, L. Sun and A. Zhang, *Fuel*, 2015, **139**, 232; (*d*) S. Wu, X. Yao, L. Zhang, Y. Cao, W. Zou, L. Li, K. Ma, C. Tang, F. Gao and L. Dong, *Chem. Commun.*, 2015, **51**, 3470; (*e*) S. Yang, S. Xiong, Y. Liao, X. Xiao, F. Qi, Y. Peng, Y. Fu, W. Shan and J. Li, *Environ. Sci. Technol.*, 2014, **48**, 10354; (*f*) F. Liu, H. He, Y. Ding and C. Zhang, *Appl. Catal., B-Environ.*, 2009, **93**, 194; (*g*) Z. Wu, B. Jiang and Y. Liu, *Appl. Catal., B-Environ.*, 2008, **79**, 347; (*h*) G. Qi and R. T. Yang, *Appl. Catal., B-Environ.*, 2003, **44**, 217.
5. P. G. Smirniotis, P. M. Sreekanth, D. A. Peña and R. G. Jenkins, *Ind. Eng. Chem. Res.*, 2006, **45**, 6436.
6. W. S. Kijlstra, E. K. Poels, A. Bliek, B. M. Weckhuysen, and R. A. Schoonheydt, *J Phys. Chem. B*, 1997, **101**, 309.
7. (*a*) L. Yu, J. Ye, X. Zhang, Y. Ding and Q. Xu, *Catal. Sci. Technol.*, 2015, **5**, 4830; (*b*) X. Zhang, J. Ye, L. Yu, X. Shi, M. Zhang, Q. Xu and M. Lautens, *Adv. Synth. Catal.*, 2015, **357**, 955; (*c*) L. Xu, J. Huang, Y. Liu, Y. Wang, B. Xu, K. Ding, Y. Ding, Q. Xu, L. Yu, Y. Fan, *RSC Adv.*, 2015, **5**, 42178; (*d*) L. Yu, H. Li, X. Zhang, J. Ye, J. Liu, Q. Xu and M. Lautens, *Org. Lett.*, 2014, **16**, 1346; (*e*) L. Yu, Y. Wu, H. Cao, X. Zhang, X. Shi, J. Luan, T. Chen, Y. Pan and Q. Xu, *Green Chem.*, 2014, **16**, 287; (*f*) Y. Wang, B. Zhu, Q. Xu, Q. Zhu and L. Yu, *RSC Adv.*, 2014, **4**, 49170; (*g*) L. Yu, J. Wang, X. Zhang, H. Cao, G. Wang, K. Ding, Q. Xu and M. Lautens, *RSC Adv.*, 2014, **4**, 19122; (*h*) L. Fan, R. Yi, L. Yu, Y. Wu, T. Chen and R. Guo, *Catal. Sci. Technol.*, 2012, **2**, 1136.
8. Values in brackets were the molar ratio of Fe *vs.* Mn; The molar ratio of Mn *vs.* Ti was fixed to be 0.4 in this article; For FeO_x/TiO_2, the molar ratio of Fe *vs.* Ti was 0.4 in this article.
9. For details and high resolution spectra, please see ESI.
10. (*a*) Z. Wu, B. Jiang and Y. Liu, *Appl. Catal., B-environ*, 2008, **79**, 347; (*b*) F. Liu, H. He, C. Zhang, Z. Feng, L. Zheng, Y. Xie and T. Hu, *Appl. Catal. B-Environ.*, 2010, **96**, 408; (*c*) K. Zhuang, J. Qiu, F. Tang, B. Xu and Y. Fan, *Phys. Chem. Chem. Phys.*, 2011, **13**, 4463.
11. The Mn peaks were near to Fe peaks. But the signals for Fe(0.75)-MnO_x/TiO_2 and Fe(1.0)-MnO_x/TiO_2 were in consistence with that of the FeO_x/TiO_2, indicating that the peaks in 40°-50° scopes should be attributed to Fe signals.
12. (*a*) C. Liu, L. Chen, J. Li, L. Ma, H. Arandiyan, Y. Du, J. Xu and J. Hao, *Environ. Sci. Technol.*, 2012, **46**, 6182; (*b*) X. Tang, J. Li, L. Sun and J. Hao, *Appl. Catal., B*-Environ., 2010, **99**, 156; (c) B. Thirupathi and P. G. Smirniotis, *J Catal*, 2012, **288**, 74.
13. K. Zhuang, J. Qiu, F. Tang, B. Xu and Y. Fan, *Phys. Chem. Chem. Phys.*, 2011, **13**, 4463.
14. P. R. Ettireddy, N. Ettireddy, S. Mamedov, P. Boolchand and P. G. Smirniotis, *Appl. Catal., B-Environ.*, 2007, **76**, 123.
15. The oxidation of $^{15}NH_3$ might generate $^{15}N_2$, which had similar molecular weight to ^{14}NO and might disturb the related curve in Figure 7.
16. (*a*) F. Kapteijn, L. Singoredjo, A. Andreini and J. A. Moulijn, *Appl. Catal., B-Environ.*, 1994, **3**, 173; (*b*) G. Ramis, L. Yi, G. Busca, M. Turco, E. Kotur and R. J. Willey, *J. Catal.*, 1995, **157**, 523.

Table of Contents

Promotional effect of iron oxide on the catalytic properties of Fe-MnO_x/TiO_2 (Anatase) Catalysts for the SCR reaction at low temperatures

Shengcai Deng, Ke Zhuang, Boliang Xu, Yuanhua Ding, Lei Yu,* and Yining Fan*

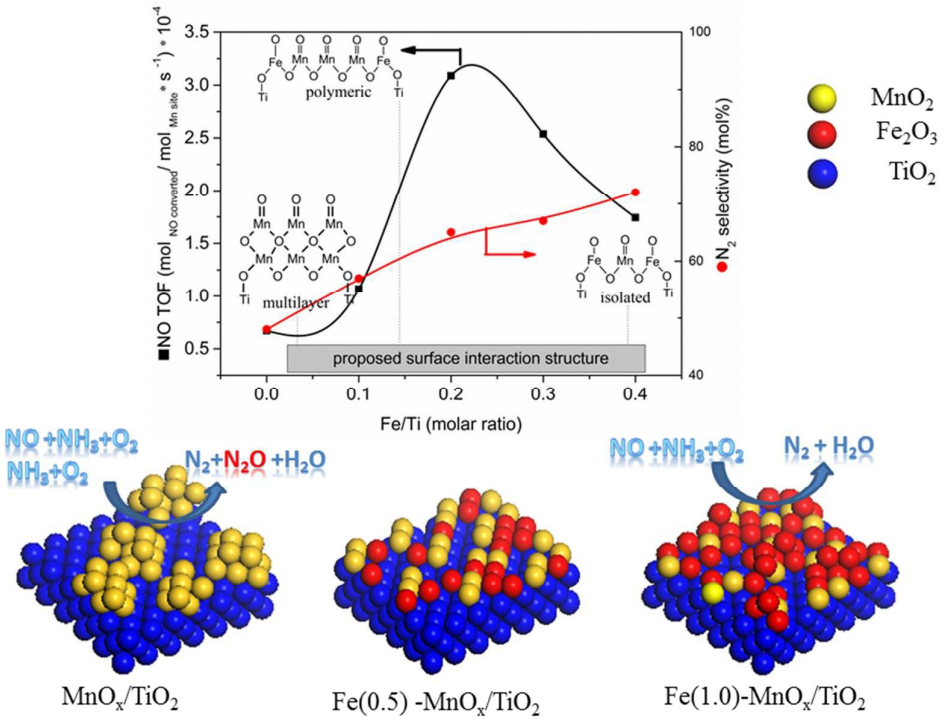

The surface ineraction of iron-improved MnO_x/TiO_2 (anatase) catalyst for the selective catalytic reduction of nitric oxide was studied by detailed experiments. It was found that iron improved the catalyst by regulating the polymerization degree and the dispersion of Mn oxide species supported on the anatase surface, which was the key factor for both the SCR activity and N_2 selectivity.